IAC–24–A6,7,10,x81057

Covariance estimation and fusion for ephemeris-only catalogues applied to the Special Perturbations Catalogue

Pietro Canal[a,b*], Alejandro Cano[a], Santiago Martínez[a], Adrián Hernández[a], Pierluigi Di Lizia[c], Diego Escobar[a]

[a] *G.M.V., Calle de Isaac Newton, 11, 28760 Tres Cantos, Madrid, Spain,*
alcano@gmv.com, samartinez@gmv.com, adrian.hernandez.for@gmv.com, descobar@gmv.com
[b] *German Aerospace Center – DLR, Institute of Space Systems, Guidance, Navigation and Control Systems, Robert-Hooke-Strasse 7, 28359 Bremen, Germany,*
pietro.canal@dlr.de
[c] *Politecnico di Milano, Aerospace Science and Technology Department, via Giuseppe La Masa, 34, 20156 Milano, Italy,*
pierluigi.dilizia@polimi.it
[*] Corresponding author

Abstract

The availability of realistic covariance information for the orbit of every Resident Space Object (RSO) contained in a catalogue is crucial for Space Situational Awareness activities, e.g., collision avoidance services. The most comprehensive of these catalogues is the Special Perturbations Catalogue (SPCAT), maintained by the U.S. 18th Space Defense Squadron. The SPCAT is the high-precision ephemeris version of the Two Line Elements RSOs catalogue, publicly available on databases such as Space Track and Celestrak. However, covariance information is not provided with the SPCAT ephemerides' mean state. So-called observed covariance values can be obtained via a comparison procedure between consecutive orbit information updates referring to the same SPCAT RSO. This paper proposes new methodologies for calculating covariance values for catalogues deprived of such information, including the application and adaptation of existing data fusion methods from the literature. The main final goal is computing covariance matrices that are more realistic and reliable than those obtained with the currently available methods. Another key objective is the integration of the new methodology in an operational environment. Computational efficiency is then a relevant factor and, consequently, the baseline method to be developed is selected and then improved taking into account such efficiency criterion. A new routine that considers the Orbit Determination epoch of each RSO ephemeris arc to coherently combine covariances based on their propagation time is developed and implemented. Two fusion methods are deployed, Covariance Intersection and Covariance Union, and the realism of the results is tested with a well-established metric, the Mahalanobis distance and its fitting of the Chi-square distribution according to appropriate Empirical Distribution Function tests such as Cramer-von Mises. The realism of the combined covariances is validated against precise ephemeris of LEO Sentinel satellites. While Covariance Intersection is proved inadequate as a stand-alone fusion method due to the characteristics of the SPCAT observed covariances, Covariance Union provides covariance values that are consistently more realistic than the ones obtained with the baseline method.

Keywords: covariance realism, data fusion, Special Perturbations Catalogue, Mahalanobis distance

Nomenclature

$\mathbf{\Delta x}$	Orbital differences set
Δx	Single element of an orbital differences set
$\mathbf{A}$	Generic matrix
$\mathbf{C}$	Covariance matrix
$\mathbf{I}$	Identity matrix
$\mathbf{x}$	6-dimensional position and velocity state vector
ω	Weight parameter
C	Single element of a covariance matrix
$chol[\cdot]$	Upper triangular Cholesky decomposition operator
d_M	Mahalanobis distance
D_{KS}	Kolmogorov-Smirnov test metric
F	Memory factor
J_{CvM}	Cramer-von Mises test metric
$max\{\cdot\}$	Element-wise maximum operator
N	Number of days of data storage for raw covariances computation
n_{COV}	Number of previously computed raw covariance arcs used for fusion methods

t	Absolute epoch
x	6-dimensional position and velocity state vector

Acronyms/Abbreviations

AGG	Aggregated
CA	Collision Avoidance
CDF	Cumulative Distribution Function
CI	Covariance Intersection
CU	Covariance Union
CvM	Cramér–von Mises
GCRF	Geocentric Celestial Reference Frame
KS	Kolmogorov-Smirnov
OD	Orbit Determination
PDF	Probability Density Function
POD	Precise Orbit Determination
RSO	Resident Space Object
S3A	Sentinel 3A satellite
S6A	Sentinel 6A satellite
SPCAT / SP	Special Perturbations Catalogue
SSA	Space Situational Awareness

1. Introduction

Tens of thousands of man-made tracked objects larger than 10 cm orbit the Earth [1], with the population size of objects larger than 1 mm estimated to be exceed 100 millions in number. These artificial satellites are named Resident Space Objects (RSOs). One of the main objectives of Space Situational Awareness (SSA) activities is the build-up and maintenance of RSOs catalogues. The availability of an updated and accurate catalogue is of the utmost importance for services such as Collision Avoidance (CA), with the goal of maintaining safety in the orbital regions of the Earth and preventing the initiation of a cascade-like process of in-orbit fragmentations and collisions between satellites [2]. The most comprehensive of these catalogues is the Special Perturbations Catalogue (SPCAT), maintained by the U.S. 18th Space Defense Squadron. Equally important as the knowledge of an RSO mean estimated orbit is the availability of the uncertainty associated to such orbit. The most commonly employed uncertainty representation in the SSA domain is the covariance matrix under Gaussian and linear assumptions, in a compromise between accuracy and efficiency. The SPCAT catalogue does not provide any information of this sort. Covariance plays a key role in contexts such as catalogue maintenance or Probability of Collision computations that find applications, e.g., in CA services. Achieving covariance realism means that the estimated mean and covariance are the true mean and covariance, respectively. Observed covariance values can be obtained via a comparison procedure between consecutive orbit information updates referring to the same SPCAT RSO.

The scope of the work is the estimation of covariance data as realistic as possible for the SPCAT objects. The intent is to compare available methodologies and select, as a development baseline, the one which is most suitable for operational purposes for a catalogue with such a high number of object entries as the SPCAT. Once this baseline selection is made, an analysis regarding the current status of the provided covariance data is to be performed. The idea is then to develop a procedure pertaining to the framework of sensor and data fusion, where information from different sources referring to the same object of interest is combined with different methods. In this case, the different data sources would be covariance matrices referring to the same object but computed on different days. The objective is then to improve the realism of the obtained covariances with respect to the baseline ones. An assessment of the covariance realism of the current methodologies for RSOs catalogues that do not provide it has never been performed, to the author's knowledge. Hence, the realism of the covariance data obtained with the newly modified methodology is tested with suitable metrics and statistics. The tests are conducted also for the baseline methodology, to evaluate the improvement. Note that the SPCAT updates do not contain information regarding planned orbital manoeuvres by active objects. Therefore, the covariance realism assessments and tests for the new methodology need to be performed on catalogue objects that have a sufficiently wide timespan of manoeuvre-free orbital motion.

2. State of the Art - *Focusoc*

Different methodologies for covariance computation of RSOs catalogues that do not provide it are employed in the framework of services provided by GMV. In the ***Focusoc*** service, the main performed task consists of collision risk assessment and warning to operators receiving the service. Most public information regarding ***Focusoc*** and its SPCAT covariance computation methodology is retrieved from [3] unless specified.

Nominally, SPCAT orbit information of an object is updated once per day. An orbit fitting process to ***Focusoc*** orbital models is then performed, and orbit data is propagated backward and forward, extending the time span of the unprocessed SPCAT ephemeris. The fitted orbit data from up to previous N days is stored to perform the covariance computation. The procedure is depicted in Fig. 1,

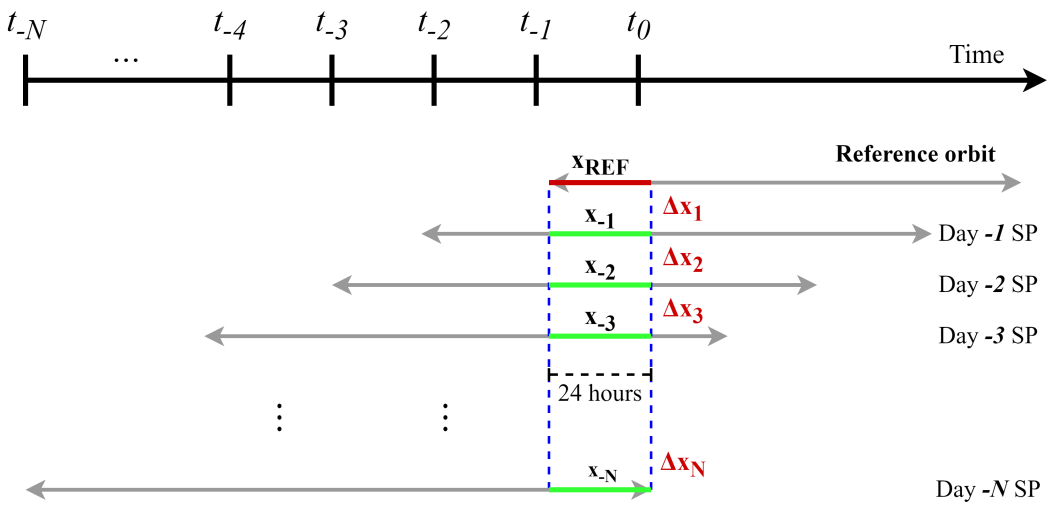

Fig. 1. ***Focusoc*** orbital differences procedure

with t_0 being the day and time of execution of the program. The most recent SPCAT orbit is the one with the most updated information, and can be taken as the reference. Given this reference 24-hour portion of the orbit state vector set $\mathbf{x_{REF}}$ - highlighted in red in Fig. 1 - N sets of orbital differences are computed against data referring to the same period from SP ephemeris published the previouss day with respect to the reference orbit, $\mathbf{x_{-i}}$ (in green) with $i = 1, ..., N$. Nominally, i.e., in the case where the SPCAT orbit was updated on day t_0 with respect to the previous one, the state vector $\mathbf{x_{-i}}$ is the result of additional i days of propagation. The sets of orbital differences along n epochs in the 24-hour interval are obtained as follows:

$$\begin{aligned} \mathbf{\Delta x_1}^{6\times n} &= \mathbf{x_{REF}}^{6\times n} - \mathbf{x_{-1}}^{6\times n} \\ \mathbf{\Delta x_2}^{6\times n} &= \mathbf{x_{REF}}^{6\times n} - \mathbf{x_{-2}}^{6\times n} \\ &\vdots \\ \mathbf{\Delta x_N}^{6\times n} &= \mathbf{x_{REF}}^{6\times n} - \mathbf{x_{-N}}^{6\times n} . \end{aligned} \quad [1]$$

The differentiation is performed in the TNW local reference frame [4]. The process is repeated up to day t_{-N}, obtaining N sets of 24-hour orbital differences. These sets are then subdivided into smaller segments, referred to as boxes. The employed nominal time width for a box is 6 hours, granting four covariance matrices per day. Figure 2 depicts the division of each 24-hour set of orbital differences into boxes . Given an orbital differences box $\mathbf{\Delta x}^{6\times q}$ referring to q different epochs, Equation 2 and Equation 3 describe the computation procedure for one covariance matrix $\mathbf{C}^{6\times 6}$ from a single orbital difference box.

The extra-diagonal terms are computed as:

$$C_{k,r} = \frac{1}{q}\sum_{i=1}^{q}[\Delta x_{i,k}\Delta x_{i,r}] \quad [2]$$

while for diagonal terms a Root Mean Square expression is employed:

$$C_{k,k} = \left(\sqrt{\frac{\sum_{i=1}^{q}(\Delta x_{i,i})^2}{q}}\right)^2 \quad [3]$$

These **C** matrices computed daily, before any kind of aggregation or fusion, will be referred to as raw covariances. The evolution of a specific type of covariance matrix over time for a single object is a covariance arc. The first computed 24-hour box set, originated from the orbital difference between $\mathbf{x_{REF}}$ and $\mathbf{x_{-1}}$, constitutes the covariance associated to the first 24 hours of the reference orbit. The second box set gets associated to the period from 24 to 48 hours of the reference orbit start, and further in time for the next box set, as depicted in Fig. 3.

Care should be taken when considering the raw covariance data for objects on high-eccentricity orbits. The magnitude of the velocity vector changes considerably from perigee to apogee in orbits with high values of orbital eccentricity. Therefore, the associated position covariance magnitude is also expected to oscillate considerably along an orbital period. Needing to group together several hours of orbit data for the computation of one single covariance matrix, this expected behaviour is difficult to retain in the computed uncertainty, where instead an average value is obtained over an entire box-width.

Raw covariance values, obtained as described in Equa-

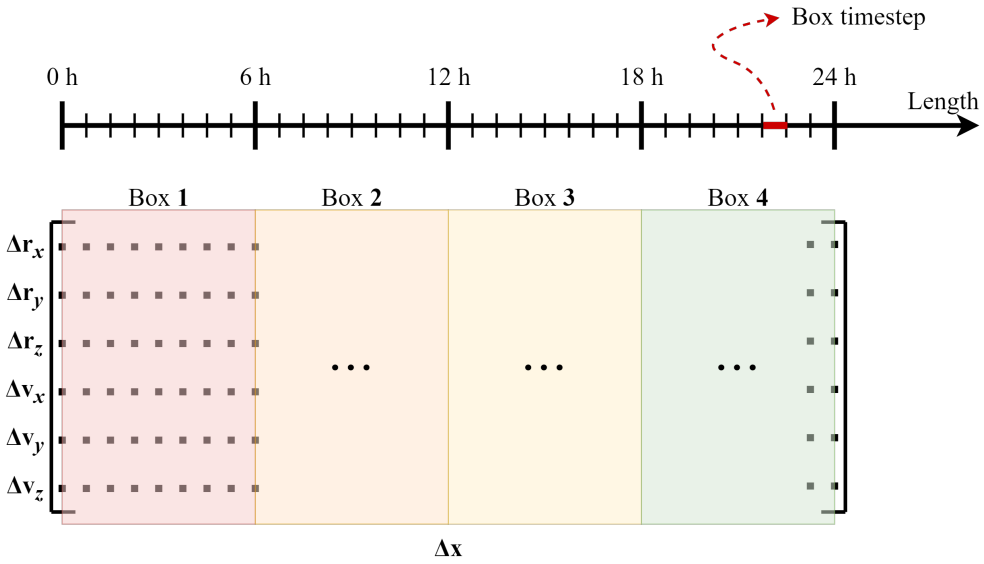

Fig. 2. Orbital differences set $\mathbf{\Delta x}$ division into boxes

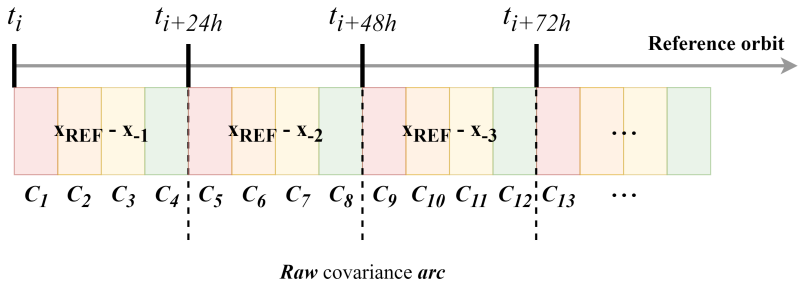

Fig. 3. Build-up of a raw covariance arc with matrices from single boxes

tion 2 and Equation 3, are not guaranteed to be successfully computed at every box-width step. Data gaps in the catalogue are possible, and several data filters are in place.

Therefore, in order to always be able to provide gap-free covariance arcs, ***Focusoc*** stores and provides aggregated (AGG) covariance matrices $\overline{\mathbf{C}}$ employing the use of a memory factor F, where superscript 0 refers to the current process and -1 to the previous day iteration:

$$\overline{C}^{0}_{k,r} = \frac{\overline{C}^{-1}_{k,r} F + C^{0}_{k,r}}{1+F} \qquad [4]$$

Evidently, this aggregation method is purely algebraic, not accounting for the covariance matrices' physical interpretation, i.e., the associated ellipsoid. Other alternatives are considered, but the ***Focusoc*** method is the only one that allows daily processing of data from a catalogue as extended as the SPCAT. Hence, a new solution, aiming to combine the computational efficiency of ***Focusoc*** while at the same time improving the associated covariance realism, is then proposed and tested in the following sections of this work.

3. Methodology

3.1 Propagation time and fusion process

After the analysis of the currently available data is conducted, new procedures and established data fusion methods for combining the raw covariance information are implemented for the novel and improved part of the methodology. If each day of raw covariance data is treated as a different data source, then fusion algorithms such as Covariance Intersection and Covariance Union can be applied.

For the new methodology, assuming the process is run for a particular object on day t_0, the correspondent Orbit Determination (OD) epoch of the reference orbit is associated with the resulting raw arc. Likewise, all the previous n_{COV} raw arcs that are retrieved to be fused have an asso-

ciated OD epoch. This step allows fusing previous arcs by comparing propagation time. The use of the local TNW frame is what allows the fusion to take place, as even with coherent propagation times, covariance matrices pertaining to different absolute epochs would exhibit completely different proportions in inertial frames such as GCRF [4].

The covariance arcs are fused in a recursive fashion. The most recent available raw arc on day t_0 is fused with the first of the n_{COV} previous raw arcs. Once this fusion is completed, the resulting arc is then fused with the second of the previous n_{COV} raw arcs; the fusion iterations continue until all n_{COV} previous raw arcs are scanned and fused. Although the n_{COV} parameter is user-configurable, its selection is very relevant for the realism of the output data, and its tuning is investigated in Section 4.

Given the nominal operation procedure of the SPCAT, the state from the most recent published orbit is expected and, therefore, assumed, to provide the best accuracy. Thus, no state fusion is performed in this work since the most accurate state could only be mixed with others from orbits of previous days that, at the same absolute epoch, have been propagated longer and consequently have accumulated a greater propagation error.

3.1.1 Covariance Intersection

Covariance Intersection (CI) is an efficient and extensively used algorithm in multi-sensor data fusion. The method considers the intersection of two or more Gaussian distributions individually characterized by some mean and covariance.

The Covariance Intersection algorithm provides a suboptimal solution to combining the mean and covariance obtained from multiple tracking solutions. CI is suboptimal because it does not enable the full extraction of the information contained within each tracking solution. However, this comes with the relevant benefit of not requiring any knowledge of the correlation or interdependence of each solution [5]. This is particularly relevant for this work, as no information regarding the correlation of measurements used for the OD of each object of the SPCAT is provided by the 18th SDS.

The algorithm is retrieved from [6]. $\mathbf{C_1}$ and $\mathbf{C_2}$ are the two covariance matrices to fuse. The CI combination formula for the fused matrix is:

$$\mathbf{C_{CI}} = \left(\omega(\mathbf{C_1})^{-1} + (1-\omega)(\mathbf{C_2})^{-1}\right)^{-1}, \qquad [5]$$

where $\omega \in [0,1]$ is optimized according to some criteria. Analytical solutions for ω are available if the cost function is chosen to minimize the determinant of $\mathbf{C_{CI}}$ and if the matrices are of size 3×3. Considering only the position sub-block of the 6×6 position-velocity covariance matrix is acceptable, since the CA methods employed in ***Focusoc***, and more in general most CA methods, utilize only the position 3×3 covariance matrix. Therefore, the method is implemented with the cost function to minimize equal to the determinant of $\mathbf{C_{CI}}$ for 3×3 position covariance matrices. Figure 4 represents a 2-D CI fusion.

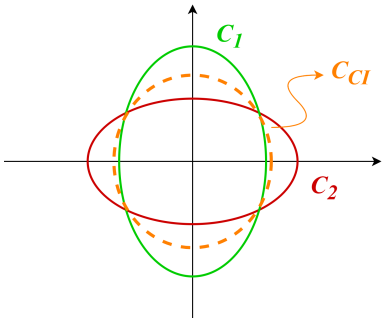

Fig. 4. 2-D CI with determinant minimization

In general, because of its nature of intersecting information, CI is not fault-robust in case of inconsistent or contradictory information to be fused, which could be the case with the raw covariance arcs at hand. In [7], a comprehensive overview of fault-tolerant methods for data fusion is presented. An alternative method mentioned in this source has been investigated and is presented next.

3.1.2 Covariance Union

The Covariance Union (CU) method is particularly suited in the occurrence of inconsistent information, i.e., mean state and associated covariance data that refer to the same object but are contradictory. The resulting fused mean and covariance solve the inconsistency, in a process referred to as deconfliction [7]. If the inconsistencies mentioned above are present, this method is to be preferred to CI. The considerations regarding state fusion made in Section 3.1 hold true. Therefore, the CU algorithm is presented and used in a simplified version, fusing the covariance matrices exclusively. According to the procedure from [8], being $\mathbf{C_1}$ and $\mathbf{C_2}$ the two matrices to fuse, then matrix $\mathbf{S}$ is defined as:

$$\mathbf{S} = chol[\mathbf{C_2}]\,, \qquad [6]$$

defining then:

$$\mathbf{M} = \left(\mathbf{S}^{-1}\right)^T \mathbf{C_1} \mathbf{S}^{-1}\,. \qquad [7]$$

Let $\mathbf{V_M}$ and $\mathbf{E_M}$ be the matrices of orthonormal eigenvectors and eigenvalues of $\mathbf{M}$ respectively. Then, the fused matrix is:

$$\mathbf{C_{CU}} = \mathbf{S}^T \mathbf{V_M}\, max\{\mathbf{E_M}, \mathbf{I}\}\, \mathbf{V_M}^T \mathbf{S}\,. \qquad [8]$$

The fusion method is applied recursively on the selected raw arcs, as described in Section 3.1.

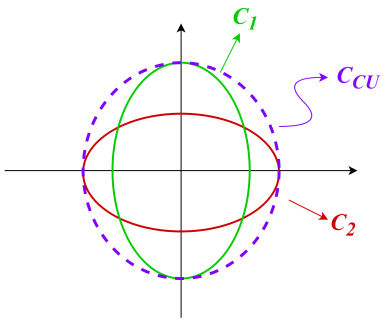

Fig. 5. 2-D CU

A 2-D ellipse representation of the fusion method is provided in Fig. 5. One relevant consideration is to be made that could be one of the contributing factors in CU outperforming CI consistently in terms of covariance realism. Recalling the nominal orbital differences procedure for the raw arc computation from Section 2, it is noted that for the first 3-4 days pairs of orbital differences, the reference orbit at t_0 very likely has shared a significant number of observations with the ones up to 3-4 previous days for its OD process, exhibiting correlation. This leads to unrealistic smaller sizes of the observed covariances. Hence, if a systematic undersizing is observed in the raw arcs, this problem needs to be tackled a-posteriori, i.e., in the fusion process. A method such as CU, that enlarges the covariance volume with respect to the inputs, would then be more suitable for the case at hand compared to CI.

3.2 Covariance realism assessment

The metric employed to evaluate how realistic the obtained covariances are is the Mahalanobis distance. It is a well-known statistical figure that describes how far a state $\mathbf{x}$ is from a specific reference $\mathbf{x_{REF}}$, projected into the covariance space [9, 10]. For the sake of validation, precise ephemeris provided by GMV Precise Orbit Determination (POD) products are used as reference orbits. These are orbits with an accuracy below the centimetre of ESA's Sentinel satellites processed by GMV. The uncertainty of SPCAT orbits is expected to be orders of magnitude higher than the one of the POD orbits. Hence, the covariance of the reference can be neglected, with the squared Mahalanobis distance being computed then as:

$$d_M{}^2 = (\mathbf{x_{SP}} - \mathbf{x_{POD}})^T (\mathbf{C_{SP}})^{-1} (\mathbf{x_{SP}} - \mathbf{x_{POD}}) \quad [9]$$

The associated covariances can be considered realistic if they are representative of the orbital difference between each SPCAT orbit and the POD orbit. Analogously, in the covariance space, if the covariance is representative of the orbital difference, the $d_M{}^2$ distribution of the orbital differences should follow a χ^2 distribution under Gaussian assumptions [10]. Thus, Empirical Distribution Function statistics can be computed to determine whether the observed Mahalanobis distances follow the χ^2 distribution. The employed analytical formulas for computations of such metrics are found in [10].

Cramer-von Mises This test establishes a quadratic metric J_{CvM}, based on the squared differences between the observed empirical distribution and the theoretical one. The null hypothesis of this test is that the candidate distribution belongs to the χ^2 distribution. Such a hypothesis can be rejected with a 99.9% confidence level if the metric reaches values above 1.16 approximately. For a more robust applicability of such metric, upper tail correction factors, as described in [11] can be applied [10].

Kolmogorov-Smirnov This test establishes a supremum metric D_{KS} that consists in the maximum vertical difference between the empirical and theoretical CDFs. In this case, the null hypothesis can be rejected for metric higher than 1.95 at same 99.9% confidence level. And, as for Cramer-von Mises, tail correction factors can be applied [10].

4. Results & Discussion

4.1 Test outline

Fused covariance arcs for Sentinel satellites with sufficient available POD data are generated with both fusion methods. The orbital differences between the SPCAT and the POD orbits corresponding to the obtained covariance arcs are then computed. Afterwards, the distribution of squared Mahalanobis distance is obtained as per Equation 9. This procedure is executed for the three types of arcs: raw, aggregated and fused. SPCAT and POD orbit data is selected sufficiently far from manoeuvres epochs, in order not to impact the orbital differentation procedure.

In general, realistic covariances are not easy to obtain due to the numerous uncertainty sources in dynamical or measurements models, which require proper uncertainty quantification techniques, as detailed in [10, 12, 13]. The results will be satisfactory if fit metrics for the fused arcs are consistently lower than the ones of aggregated arcs. This achievement would mark the improvement in covariance realism of the new solution, which has been set as one of the key objectives of this work.

4.2 Initial fusion results with CI

The initial tests are conducted for CI on Sentinel-6A (S6A) data, being this the POD satellite with the biggest time interval between maneouvres and, therefore, with more data available. This satellite is placed on a quasi-circular orbit of 1336 km height.

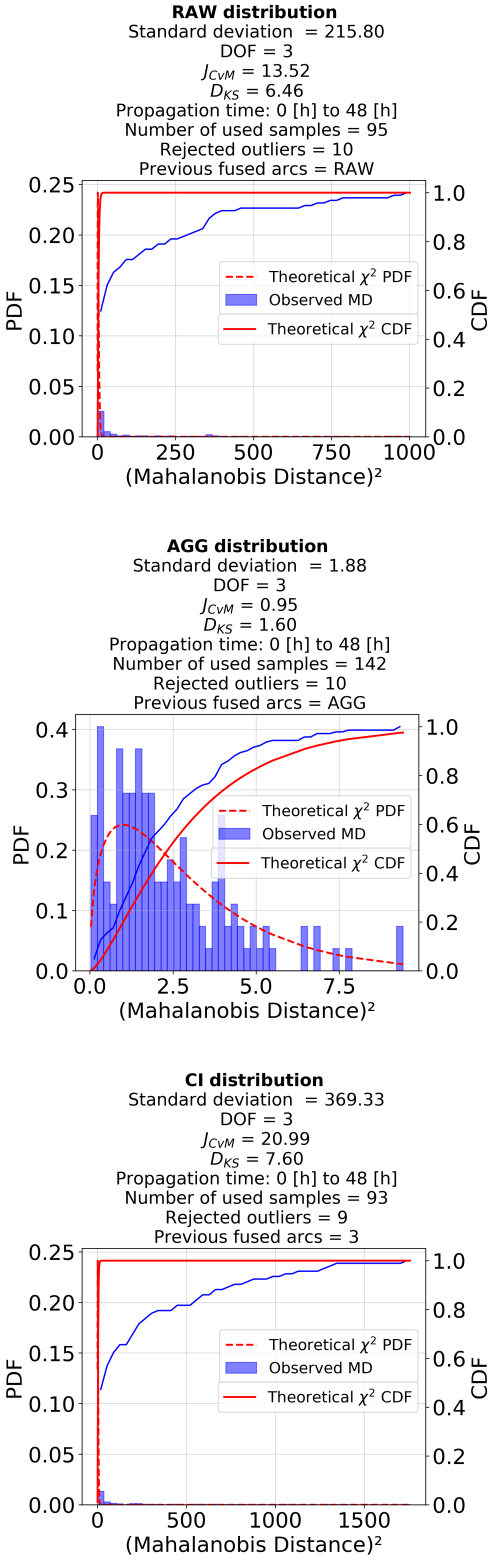

Fig. 6. S6A ${d_M}^2$ [0-48] hours

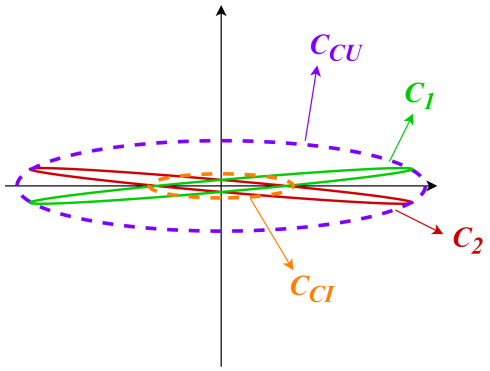

Fig. 7. 2-D fusion of covariance matrices in TNW frame

Due to the limited amount of data available, different propagation times are grouped to obtain a sufficient number of available samples for the statistical tests metrics to be significant. For these initial CI results, 8 box-width are grouped together, resulting in propagation intervals of 48 hours. No propagation time further than 6 days is analysed, given that Sentinel satellites reside in LEO, a region where even refined OD and propagation models significantly worsen their accuracy after the 7-day mark. The intent is to conduct the tests with a maximum 3-day width per propagation interval, or less as long as the amount of available samples is high enough to maintain significance from a statistical viewpoint. The reason for this is to be possibly able to detect a shift in the covariance trend after the first 3-4 days of propagation because of the correlation problem between SPCAT orbits mentioned in Section 3.1.2. Here, the number of previous raw arcs to fuse with the current one is kept constant, with $n_{COV} = 3$. Empirical evidence, as per [11], suggests that Cramer-von Mises is often more powerful than Kolmogorov-Smirnov test for a broad class of alternative hypotheses, so the output metrics are considered accordingly.

From the initial results in Fig. 6, important considerations can be made, particularly on the realism of the raw and CI-fused data. Raw arcs appear to be associated with extremely high Mahalanobis distances with respect to the χ^2 distribution. When considering the ${d_M}^2$ formulation from Equation 9, it is then clear that this implies greatly undersized covariance values. It is, most likely, a confirmation of the hypothesis on the influence of correlation between SPCAT orbits made in Section 3.1.2. For the CI results, in terms of both the J_{CvM} and D_{KS} test metrics, the performance is even worse than the raw ones. Such a behaviour appears to be a confirmation on the considerations made in Section 3.1.1 on the use of CI in fusing covariance data that is likely already undersized. In addition, if the physics of the problem of combining covariances in

TNW frame is considered, a typical fusion scenario between two covariance matrices (once again represented as 2-D ellipses for easier visualization) is displayed in Fig. 7.

It is well established that the velocity-aligned along-track component T in a TNW local frame representation is the one characterized by the greatest uncertainty, usually 1 or 2 orders of magnitude higher than the normal and cross-track components. Hence, a realistic TNW covariance ellipsoid will be "needle-shaped" and greatly elongated in T direction. Therefore, as displayed in Fig. 7, with even a slight misalignment in the principal axes orientation of the two ellipsoids to be fused, the resulting CI fused ellipsoids are significantly reduced in size.

4.3 Final fusion results with CU

After having ascertained that standalone CI is not adequate for the scenario at hand, the focus of the work shifted to CU. For this reason, more comprehesive results are only shown for CU from this point onwards. Tests are now also conducted with Sentinel-3A data, which resides in a sun-synchronous orbit at 814.5 km altitude. For CU-fused distributions, graphs and tables are reported for the value of n_{COV} yielding the lowest test metrics.

Several input parameters of the covariance computation and fusion process, such as the box-width, were varied to detect elevated sensitivity. By far, the input parameter affecting the most the tests' metrics and the fused covariance realism is found to be number of previous raw arcs to fuse, n_{COV}. Hence, this parameter is varied between 2 and 4 for all possible propagation time intervals, and its impact on the final results is analysed.

4.3.1 S6A

CU Graphs in Fig. 8 and Fig. 9 are reported for the value of n_{COV} yielding the lowest J_{CvM} metric, for the [0,24) and [96,120) hours intervals. Table 1 reports the test metrics for the six intervals. Note that even fused arcs could still have gaps in the 6-hour progression scheme, or it could be that only one matching covariance matrix value is found for a specific propagation time, and so no fusion is performed for that propagation epoch. To analyse more accurately the actual performance of the fusion methods, only Mahalanobis distances computed with a covariance value that had at least one successful fusion performed are input to the statistical test. The n_{COV} values in Table 1 are then reported with a "-" sign, as to indicate the maximum number of fusions performed for the samples in that interval, while there are samples for which less fusions have been performed.

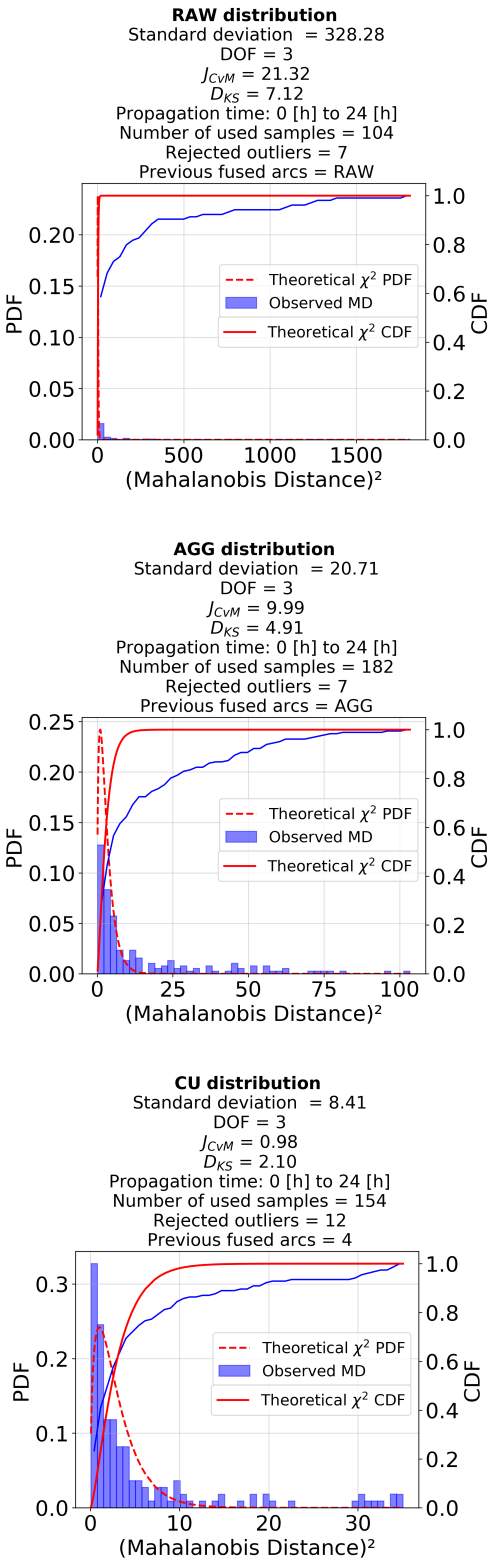

Fig. 8. S6A ${d_M}^2$ [0-24] hours

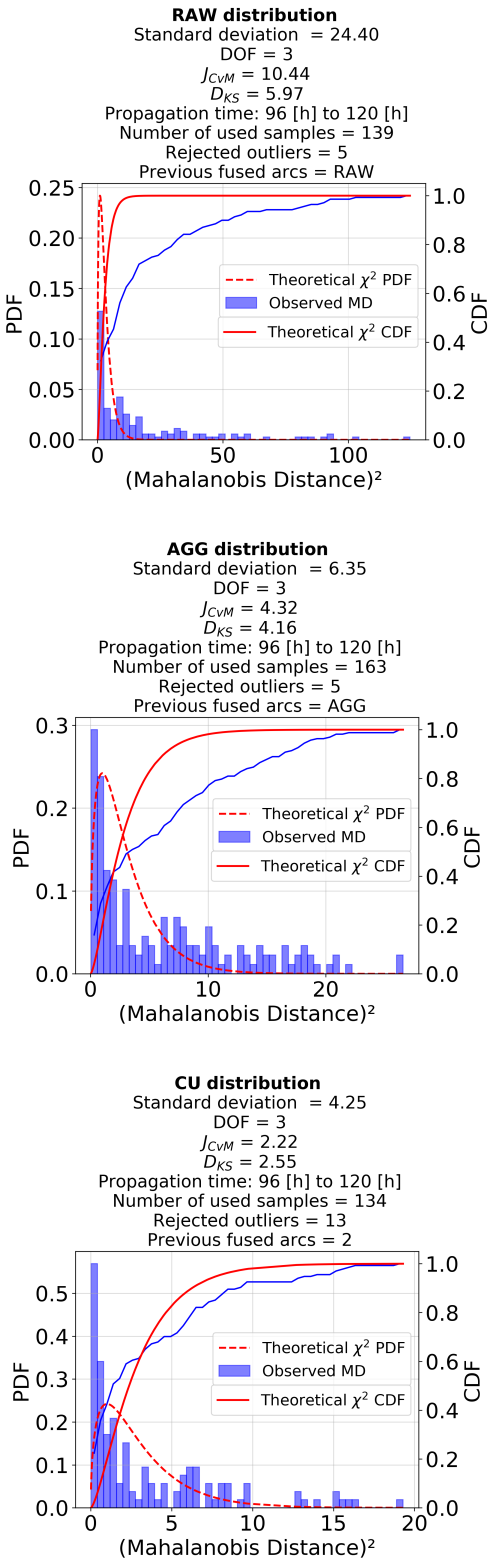

Fig. 9. S6A $d_M{}^2$ [96-120] hours

Table 1. S6A test metrics for CU and AGG distributions

Propagation interval [h]	n_{COV}	J_{CvM} CU	J_{CvM} AGG	D_{KS} CU	D_{KS} AGG
[0, 24)	4-	**0.98**	**9.99**	**2.10**	**4.91**
[24, 48)	2-	**1.32**	**3.99**	**2.35**	**3.60**
[48, 72)	2-	**1.59**	**2.47**	**2.14**	**3.06**
[72, 96)	2-	**2.08**	**3.87**	**2.90**	**3.78**
[96, 120)	2-	**2.22**	**4.32**	**2.55**	**4.16**
[120, 144)	2-	**2.32**	**3.37**	**2.36**	**3.71**

From Fig. 8 and Fig. 9, it is clear that the CU samples follow the theoretical χ^2 distribution better than the AGG ones. Consequently, the test metrics in Table 1 show that CU, as opposed to CI, consistently yields lower, and therefore, more realistic, goodness-of-fit metrics compared to the ones of the aggregated distributions. For the first 24 hours interval, i.e., [0, 24), the best results are obtained with $n_{COV} = 4$. Then, the optimum choice is 2 for the test case at hand from the [24, 48) interval onwards. These seem to be a further confirmation of the impact that the correlation between the first 3-4 orbits of the SPCAT has on the covariance computation. As the correlation is reduced going further in propagation time, less previous raw arcs are required to be fused to obtain a more realistic, not undersized fused covariance arc.

The evolution of the raw distributions supports this claim further. Indeed, a significant reduction in the dispersion of the Mahalanobis distances is observed from [96, 120) hours interval onwards, as shown in Fig. 9. This can be explained if the correlation between the reference orbit and the ones that are more than 3-4 days apart from it is no longer present, resulting in raw less undersized covariance matrices and lower $d_M{}^2$ values.

4.3.2 S3A

With the same month span of available data but much shorter time gaps between manoeuvres, propagation intervals have to be increased to a 72-hour length to obtain sample distribution sizes comparable to the one for S6A. As already mentioned, tests on a lower LEO altitude satellite are of particular interest. However, data scarcity is a significant problem for the satellite at hand that can only be solved with several months of increased covariance information storage in the future. Therefore, the outcomes for S3A test are reported for completeness, but care should be taken when considering them compared to the more comprehensive test with S6A. As done for S6A in Section 4.3.1, CU Graphs in Fig. 10 and Fig. 11 are reported for the value of n_{COV} yielding the lowest J_{CvM} metric, for the [0,72) and [72,144) hours intervals.

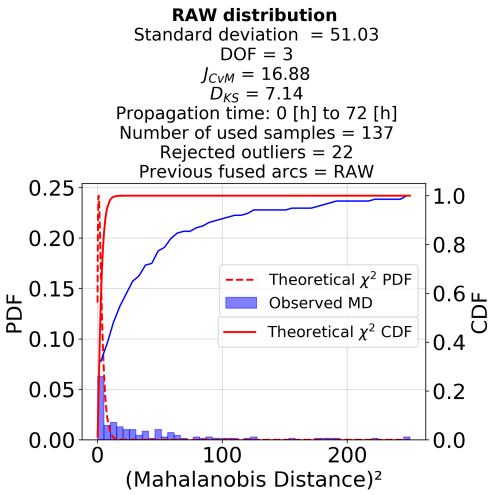

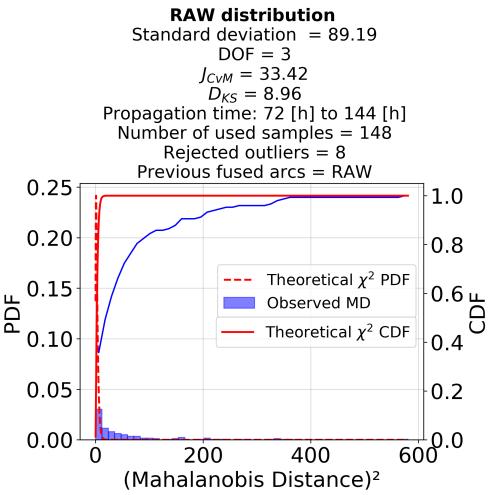

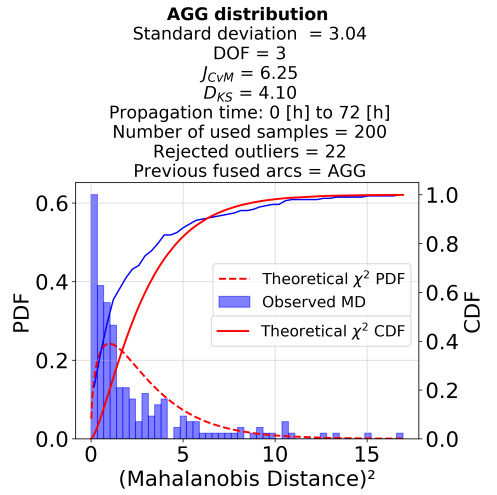

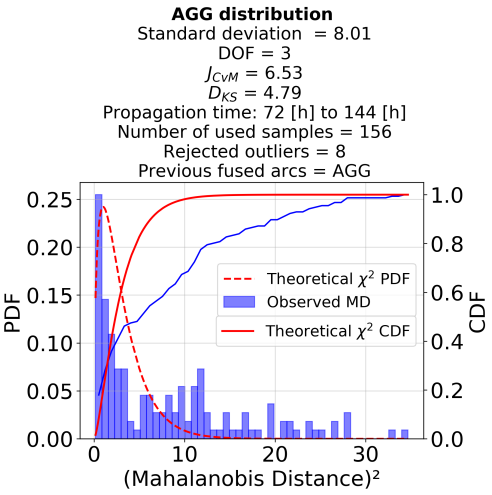

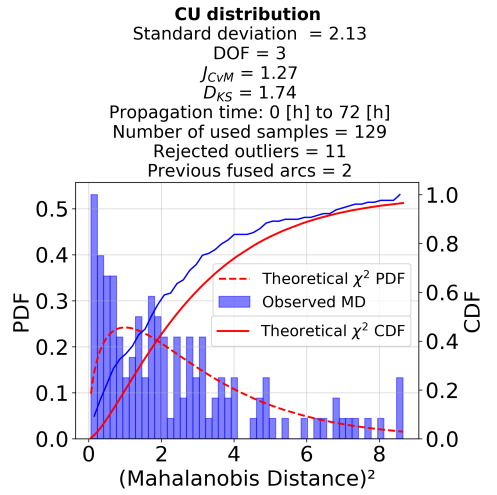

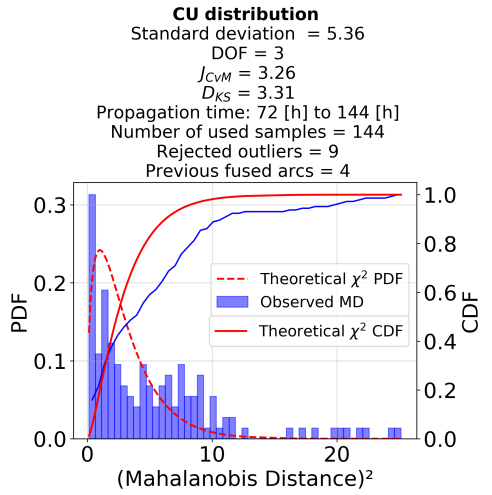

Fig. 10. S3A $d_M{}^2$ [0-72] hours

Fig. 11. S3A $d_M{}^2$ [72-144] hours

Table 2. S3A test metrics for CU and AGG distributions

Propagation interval [h]	n_{COV}	J_{CvM}		D_{KS}	
		CU	AGG	CU	AGG
[0, 72)	2-	**1.27**	**6.25**	**1.74**	**4.10**
[72, 144)	4-	**3.26**	**6.53**	**3.31**	**4.79**

From the Fig. 10 and Fig. 11 graphs, it is inferred that the raw covariances are again unrealistic and greatly undersized. For S3A, the trend as propagation time progresses seems to be the opposite as S6A. Indeed, the dispersion of the squared Mahalanobis distances raw distributions increases from [0, 72) to [72, 144) hours. Even if this could seem an apparent contradiction to the statement regarding the removal of correlation between orbits made in Section 4.3.1, it very likely is not. First, only two different distributions are available to analyse for each arc type, so it is difficult to establish a clear trend. Secondly, the increased undersizing of the covariances in the [72, 144) hours range even if the influence of correlation between orbits should be greatly reduced, could be explained by an increased uncertainty in the real position of the object, i.e., increased orbital differences magnitude between the SPCAT and the POD reference orbits. S3A is located at a lower altitude than S6A, where atmospheric drag starts to have a larger influence in the orbit dynamics. Then, unless specific uncertainty quantification measures are taken, the covariance growth is not expected to match the propagation errors, leading to an overall increase in the Mahalanobis distance. Hence, the accuracy of the propagation models used for SPCAT orbits is expected to worsen considerably earlier than for S6A, characterized by smoother and more linear dynamics. Nonetheless, test metrics are still considerably lower for CU in Table 2 as compared to the baseline processes, where the consideration on the "-" sign for the n_{COV} values is the same as made for Table 1 in Section 4.3.1.

5. Conclusions

After an initial analysis of the available data from the Special Perturbations Catalogue, a new time management process taking into account the OD epochs of each orbit has been implemented building upon the covariance computation process from orbital differences embedded in the ***Focusoc*** service by GMV. Two data fusion methods, Covariance Intersection and Covariance Union, have been adapted for the scenario at hand and implemented for combining different covariances to increase the realism of the output matrices. The adopted metric for assessing the realism of the newly fused data is the squared Mahalanobis distance. Such an assessment has been performed by testing the Mahalanobis distance distributions computed with the fused covariance data against the baseline aggregated one of ***Focusoc*** with two well-proven goodness-of-fit statistics, the Cramer-von Mises and Kolmogorov-Smirnov ones.

Tests were conducted on data of two LEO satellites for which precise reference orbits to be compared with the SPCAT ones are available, S6A and S3A. It is worth highlighting that no simulated data has ever been used during the course of this work. CI has proved to be not suitable to be used as a stand-alone fusion method, given the underlying physics of the problem of combining covariances in the local TNW frame and the systematic undersizing of covariances due to the correlation between SPCAT orbits that are up to 3-4 days apart. Instead, CU has consistently provided lower goodness-of-fit metrics compared to the baseline aggregated distributions, providing more realistic results. Therefore, the initially set scope of this work can be considered achieved.

Possible future developments and improvements can be planned. The fusion procedure can be made more flexible, ensuring that each covariance matrix of the current *raw* arc gets an actually successful number of user-configurable n_{COV} fusion iterations. Currently, n_{COV} previous raw arcs are always loaded into memory. However, due to possible gaps in these types of arcs, some epochs of the new fused arc refer to matrices that had a number of successful fusions which is less than n_{COV}.

In general, data scarcity has been a challenge for the validation of the new methodology and the comparison against the baseline aggregated one. With at least some additional months of daily-obtained and processed data, more comprehensive and representative tests can be put in place, with the goal of extending the new methodology to the entire SPCAT.

Since n_{COV} appears to be the most relevant input parameter for the realism of the result, the additional tests could also focus on trying to identify trends that would allow defining the number of previous raw arcs to fuse as a function of propagation time and not as a fixed input parameter, for optimum performance. With more available data, it is possible to reduce the propagation intervals in which to group Mahalanobis distance below 24 hours, even reaching the box-width limit of 6 hours. This could allow a more reliable optimum trend evaluation for a propagation time-dependent function definition of n_{COV}, that will likely differ based on the orbital regime at hand, given the considerable difference in the influence of orbital perturbations in the different regions of the Earth space environment.

For an even further improved realism of the covariance data, a combination of Covariance Union and Covariance Intersection could be tested. CU would still be the main fu-

sion method, but CI could be employed as an a-posteriori check in cases where there is the possibility of obtaining covariance matrices that might have a too inflated volume during the nominal CU fusion.

Acknowledgements

The corresponding author would like to mention that the results presented in this paper have been obtained as part of an internship in the Space Surveillance & Traffic Management business unit at GMV. The internship was devoted to the preparation of a M.Sc. thesis in Space Engineering, defended in May 2023 at Politecnico di Milano [14]. The corresponding author would also like to acknowledge his current employer, i.e., the Guidance, Navigation & Control department of DLR Institute of Space Systems, where this paper was finalized.

References

List of references

[1] E. S. D. Office, "Esa's annual space environment report," ESA, Darmstadt, Germany: ESA ESOC, Tech. Rep. 8, Jul. 2024.

[2] H. Klinkrad, *Space Debris Models and Risk Analysis*. Springer Berlin, Heidelberg, 2006, ISBN: 978-3-642-58351-3. DOI: 10.1007/3-540-37674-7.

[3] A. Souto Janeiro, "Analysis of precision of ephemeris for focusoc," M.S. thesis, Instituto de Migrogravedad Ignacio da Riva & GMV, Jul. 2019.

[4] D. A. Vallado, *Fundamentals of Astrodynamics and Applications*, 4th ed. Microcosm Press, 2013, ISBN: 978-1881883197.

[5] K. DeMars and J. McCabe, "Multi-sensor data fusion in non-gaussian orbit determination," in *AIAA/AAS Astrodynamics Specialist Conference 2014*, Aug. 2014, ISBN: 978-1-62410-308-7. DOI: 10.2514/6.2014-4310.

[6] M. Reinhardt, B. Noack, and U. Hanebeck, "Closed-form optimization of covariance intersection for low-dimensional matrices," in *15th International Conference on Information Fusion*, IEEE, Jul. 2012.

[7] J. K. Uhlmann, "Covariance consistency methods for fault-tolerant distributed data fusion," *Information Fusion*, vol. 4, no. 3, pp. 201–215, 2003, ISSN: 1566-2535. DOI: https://doi.org/10.1016/S1566-2535(03)00036-8. [Online]. Available: https://www.sciencedirect.com/science/article/pii/S1566253503000368.

[8] S. Reece and S. Roberts, "Generalised covariance union: A unified approach to hypothesis merging in tracking," *IEEE Transactions on Aerospace and Electronic Systems*, vol. 46, pp. 207–221, 2010. DOI: 10.1109/TAES.2010.5417157.

[9] P. C. Mahalanobis, "On the generalized distance in statistics," *Proceedings of the National Institute of Sciences (Calcutta)*, vol. 2, pp. 49–55, 1936.

[10] A. Cano, A. Pastor, D. Escobar, J. Míguez, and M. Sanjurjo-Rivo, "Covariance determination for improving uncertainty realism in orbit determination and propagation," *Advances in Space Research*, 2022, ISSN: 0273-1177. DOI: https://doi.org/10.1016/j.asr.2022.08.001. [Online]. Available: https://www.sciencedirect.com/science/article/pii/S0273117722007190.

[11] R. B. D'Agostino and M. A. Stephens, *Goodness-of-Fit Techniques*. Dekker, 1986, ISBN: 978-0824774875.

[12] A. Cano, A. Pastor, S. Fernández, J. Míguez, M. Sanjurjo-Rivo, and D. Escobar, "Improving orbital uncertainty realism through covariance determination in geo," *The Journal of the Astronautical Sciences*, 2022, ISSN: 2195-0571. DOI: 10.1007/s40295-022-00343-x. [Online]. Available: https://link.springer.com/article/10.1007/s40295-022-00343-x.

[13] A. Cano, A. Pastor, J. Míguez, M. Sanjurjo-Rivo, and D. Escobar, "Catalog-based atmosphere uncertainty quantification," *The Journal of the Astronautical Sciences*, 2023, ISSN: 2195-0571. DOI: 10.1007/s40295-023-00403-w. [Online]. Available: https://link.springer.com/article/10.1007/s40295-023-00403-w.

[14] P. Canal, "Covariance information fusion for resident space objects from the special perturbations catalogue," M.S. thesis, Politecnico di Milano, May 2023. [Online]. Available: https://www.politesi.polimi.it/handle/10589/206350.